PERGAMON

International Journal of Solids and Structures 38 (2001) 3329–3340

INTERNATIONAL JOURNAL OF SOLIDS and STRUCTURES

www.elsevier.com/locate/ijsolstr

Mechanics of damage initiation and growth in a TBC/superalloy system

M.Y. Ali, S.Q. Nusier, G.M. Newaz *

Department of Mechanical Engineering, Wayne State University, 5050 Anthony Wayne Drive, Detroit, MI 48202, USA

Received 16 September 1999; in revised form 10 March 2000

Abstract

Creep analysis was used to estimate stresses in different layers especially in bond coat and the thermally grown oxide (TGO) layer to determine the role of creep on damage initiation in the TBC system. Microcracks were observed to initiate near the bond coat/TGO interface after only a few thermal cycles. The origin of these microcracks can be attributed to the buildup of thermal stresses that may magnify due to asperity of the TGO layer and the bond coat. The TGO/bond coat interface was modeled as a rough periodic surface. Finite element calculations were conducted to determine the magnitude of stresses at the bond coat/oxide interface (modeled as a sine wave). It was found that large normal interface stresses arise at the peaks, while large shear stresses arise at the mean line of the rough interface. These residual stresses can exceed the interfacial tensile or shear strength of TGO. Effect of oxide layer growth between bond coat and Thermal barrier coating (TBC) was modeled as volume increase and subsequently as an induced pressure across the interface inside the crack. Mixed-mode fracture analysis of a thin circular delamination in an axisymmetric multi-layer circular plate was developed to assess growth.

Keywords: TBC; Superalloy system; Damage initiation

1. Introduction

Brindley and Whittenberger (1993) had analyzed stress relaxation of low-pressure plasma-sprayed NiCrAlY alloys. They studied the relaxation of three NiCrAlY alloys at temperatures of 800–1000°C and over a wide range of stresses. They showed that all three bond coat alloys relaxed quite rapidly at temperatures of 900°C and above which may have a potential to affect the TBC life. Also they showed the differences in relaxation of the three alloys which may offer a possible explanation for the differences in TBC life observed for these bond coats. Evans et al. (1997) had analyzed creep effects on the spallation of an alumina layer from a NiCrAlY coating. They showed the spallation by wedge cracking of an alumina from a flat Ni16Cr6AlY coating substrate cooled at various rates from 1100°C. They concluded that slow cooling from the oxidation temperature could lead to useful increases in the high-temperature exposure period

* Corresponding author. Tel.: +1-313-577-3843; fax: +1-313-577-8789.
E-mail address: gnewaz@eng.wayne.edu (G.M. Newaz).

0020-7683/01/$ - see front matter
PII: S0020-7683(00)00261-4

before spallation would be initiated during cooling. A quantitative determination of the stress states in a model thermal barrier coating as it cools down from the processing temperature (stress-free) to another lower temperature was studied by Chang et al. (1987). Their studies showed that the radial stresses close to the wavy interface may actually alternate between regions of compression and tension. A study conducted on crenulated fiber by Carapella et al. (1994) indicates that the stress levels present with crenulated fiber are significantly higher than for the circular fiber. A mixed-mode fracture analysis combining nonlinear thin-plate stress solutions with crack-tip elasticity results has been developed to account for local variations of G_{I}, G_{II}, and G_{III} in thin-film debond problems associated with large film deformations by Chai (1990). A shaft-loaded blister test has been developed by Wan and Mai (1995) to measure the interfacial energy of a thin flexible polymeric film adhered to a rigid substrate. Expressions have been derived which describe the critical stress and pressure necessary to rupture oxide blisters, which form on aluminum during growth of corrosion pits, by Ryan and McCafferty (1995).

Till now many researchers have addressed creep problem in TBC systems, but an assessment of the magnitude of residual stresses in different layers and their consequence in damage initiation remains unexplored. Therefore in this investigation focus will be given on the estimation of the stresses in different layers especially in bond coat and the TGO to determine the role of creep on damage initiation in the TBC system. However, the primary focus was to predict the conditions for crack initiation due to thermal residual stresses at wavy interfaces and to establish an empirical equation for these stresses. Again, though numerous efforts have been made to understand the effect of cracks on the life of TBC coated specimens, evolution and growth of the cracks still require special attention. It is now determined that in some TBC systems such as electron beam–plasma vapor deposition (EB–PVD), there is microcrack initiation. Microcracks coalesce to form major delamination cracks as reported by Nusier and Newaz (1998b). Interfacial crack in a layered disk specimen is shown in Fig. 1. An important consideration is the nature of crack growth characteristics at the TBC/bond coat interface. In a previous study by Nusier and Newaz (1998b), it was shown that a central delamination under pure thermal loading has no stress intensification at the crack tip unless the delamination is large enough to promote buckling. By investigating the issue of interfacial crack growth, the condition necessary for their growth under thermo-mechanical loading will be evaluated. The button specimen under consideration is amenable to axisymmetric modeling due to geometry. The

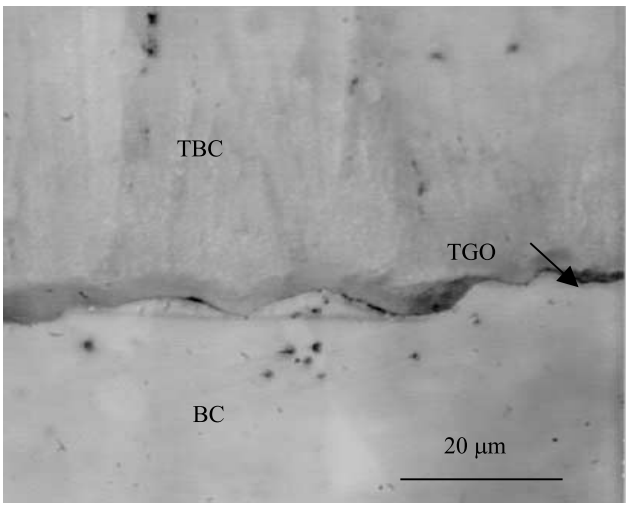

Fig. 1. An optical micrograph of a tested thermal barrier coated sample, 150 cycle. Thermal cycling temperature ranges 200–1177°C.

importance of this problem is due to the fact that in order to achieve realistic prediction of TBC spallation performance, one needs to study the interaction of various layers and interfacial cracks at high temperature.

2. Analytical and numerical modeling for creep

The geometry under consideration is a disk-type four-layer system which includes substrate, bond coat, TGO and the TBC layer. When the temperature (T) does not vary over the thickness of each layer it can be assumed that the stress and displacement due to heating also do not vary over the thickness.

2.1. Viscoplastic deformation and stresses in layers

The in-plane radial stresses as a function of time in a four-layer model of TBC disk sample can be given, for plane stress, with modification for thermal expansion as (for disk, due to symmetry, $\varepsilon_r = \varepsilon_\theta$ and $\sigma_r = \sigma_\theta$)

$$\begin{aligned}
\sigma^c(t) &= \frac{E^c}{1-\nu^c}[\varepsilon - \alpha^c(T-T_r)], \qquad \sigma^o(t) = \frac{E^o}{1-\nu^o}[\varepsilon - \alpha^o(T-T_r) + \varepsilon^o_{cr}],\\
\sigma^b(t) &= \frac{E^b}{1-\nu^b}[\varepsilon - \alpha^b(T-T_r) + \varepsilon^b_{cr}], \qquad \sigma^s(t) = \frac{E^s}{1-\nu^s}[\varepsilon - \alpha^s(T-T_r)],
\end{aligned} \tag{1}$$

where σ is the radial stress, α is the thermal expansion coefficient and T_r is the stress free temperature, the superscripts c, o, b and s refers to TBC, TGO (Al_2O_3), bond coat and substrate, respectively. The creep behavior of alumina (TGO) and the bond coat for uniaxial loading were published as follows (bond coat creep model refers to Brindley and Whittenberger (1993) and oxide creep model refers to Evans et al. (1997) and Lin and Becher (1990)

$$\begin{aligned}
\frac{d\varepsilon^o_{cr}}{dt} &= 1.08\times10^{-10}\sigma^{o^{2.3}}\exp\left(-\frac{51000}{T}\right) \quad (s^{-1}),\\
\frac{d\varepsilon^b_{cr}}{dt} &= 8.96\times10^{-15}\sigma^{b^3}\exp\left(-\frac{35840}{T}\right) \quad (s^{-1}).
\end{aligned} \tag{2}$$

But for the present case the effect of creep has been assumed in radial and tangential direction. Thus the creep strain rate for present case can be given as follows (Clarke and Barnes, 1971)

$$\begin{aligned}
\frac{d\varepsilon^o_{cr}}{dt} &= \frac{1.08\times10^{-10}}{2}\sigma^{o^{2.3}}\exp\left(-\frac{51000}{T}\right) \quad (s^{-1}),\\
\frac{d\varepsilon^b_{cr}}{dt} &= \frac{8.96\times10^{-15}}{2}\sigma^{b^3}\exp\left(-\frac{35840}{T}\right) \quad (s^{-1}).
\end{aligned} \tag{3}$$

Though the bond coat creep model refers to NiCrAlY material the same model has been assumed for the specimen used in present work with PtAl bond coat.

The equilibrium radial force equation for the four layers is

$$\sum F = \sigma^c A^c + \sigma^o A^o + \sigma^b A^b + \sigma^s A^s = 0. \tag{4}$$

Substituting Eq. (1) into Eq. (4) to solve for ε and differentiating gives

$$\frac{d\varepsilon}{dt} = \frac{-\frac{E^o}{1-\nu^o}A^o\frac{d\varepsilon^o_{cr}}{dt} - \frac{E^b}{1-\nu^b}A^b\frac{d\varepsilon^b_{cr}}{dt}}{\left(\sum_{i=c,o,b,s}\frac{E^i}{1-\nu^i}A^i\right)}. \tag{5}$$

Table 1
Material properties at 22°C, 566°C, 1149°C

Material	Young's modulus (GPa)	Poisson's ratio	Coefficient of thermal expansion ($\times 10^{-6}$/°C)
Substrate	175.8	0.25	13.91
	150.4	0.2566	15.36
	94.1	0.3224	19.52
Bond coat	137.9	0.27	15.16
	121.4	0.27	15.37
	93.8	0.27	17.48
TBC	27.6	0.25	10.01
	6.9	0.25	11.01
	1.84	0.25	12.41
Oxide	386	0.257	6
	349	0.257	8
	311	0.257	8.9

Now differentiating Eq. (1) with respect to time leads to

$$\begin{aligned} \frac{\mathrm{d}\sigma^{\mathrm{c}}(t)}{\mathrm{d}t} &= \frac{E^{\mathrm{c}}}{1-\nu^{\mathrm{c}}}\frac{\mathrm{d}\varepsilon}{\mathrm{d}t}, \qquad \frac{\mathrm{d}\sigma^{\mathrm{o}}(t)}{\mathrm{d}t} = \frac{E^{\mathrm{o}}}{1-\nu^{\mathrm{o}}}\left[\frac{\mathrm{d}\varepsilon}{\mathrm{d}t}+\frac{\mathrm{d}\varepsilon^{\mathrm{o}}_{\mathrm{cr}}}{\mathrm{d}t}\right], \\ \frac{\mathrm{d}\sigma^{\mathrm{b}}(t)}{\mathrm{d}t} &= \frac{E^{\mathrm{b}}}{1-\nu^{\mathrm{b}}}\left[\frac{\mathrm{d}\varepsilon}{\mathrm{d}t}+\frac{\mathrm{d}\varepsilon^{\mathrm{b}}_{\mathrm{cr}}}{\mathrm{d}t}\right], \qquad \frac{\mathrm{d}\sigma^{\mathrm{s}}(t)}{\mathrm{d}t} = \frac{E^{\mathrm{s}}}{1-\nu^{\mathrm{s}}}\frac{\mathrm{d}\varepsilon}{\mathrm{d}t}. \end{aligned} \tag{6}$$

Substituting Eqs. (3) and (5) into Eq. (6) gives a system of first order differential equations, which can be integrated numerically to obtain the radial stress in each layer as function of time. It may be noted that these solutions are based on mechanics of materials approach.

2.2. Finite element stress analysis

The nickel-based superalloy substrate Rene N5 had a thickness of 3.175 mm, the bond coat layer thickness is 0.036 mm, the TGO, aluminum oxide layer thickness is 0.012 mm, the TBC thickness is 0.127 mm, and the radius of the specimen is 12.7 mm. The properties of these four layers are given in Table 1. A half model was used since the specimen is axisymmetric. Eight-node axisymmetric biquadratic quadrilateral element type was used. Along the axisymmetric axis (axial), the nodes are allowed to move in the axial direction only. In the analysis, the specimen was cooled down from processing temperature (1000°C) to room temperature (25°C) and then heated to 1177°C. The specimen is held at that temperature until the stresses decay to zero and then again cooled to room temperature to investigate the effect of creep on residual stresses. A general finite element code ABAQUS was used for numerical calculations.

3. Asperity modeling

3.1. Basic formulation

The TBC coating in a button specimen as studied by Nusier and Newaz, (1998c) is in a state of biaxial compression. This residual compression stress arises because of thermal expansion mismatch. Buckling failure mode has been observed by Newaz et al., (1998a) in the EB–PVD system. Buckling mode can occur

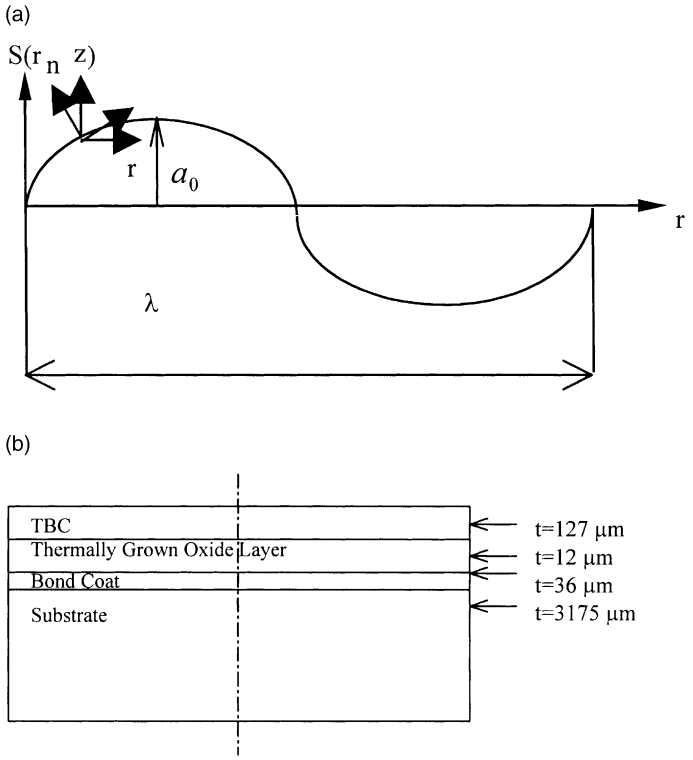

Fig. 2. (a) Bond coat/oxide interface vary in a sinusoidal shape with wave amplitude a_0, and wave length λ. (b) Dimensions of the four-layer disk specimen (radius 12.7 mm).

only in the case of a large-scale delamination (16 times TBC thickness). Thermally cycled TBC samples in air leads to the formation of an oxide layer. The interface roughness between the oxide layer and the bond coat layer leads to interfacial cracking as seen clearly in Fig. 1. Here the interface has been modeled as a sine wave (Fig. 2a) in the following form

$$S(r) = a_0 \sin\left(\frac{2\pi r}{\lambda}\right), \tag{7}$$

where $S(r)$ is the interface height, a_0 is the wave amplitude, r is the longitudinal position along interface, and λ is the wavelength. The stresses of interest are the normal and shear stresses. It should be noted that for the case of flat interface, the normal and shear stresses are zero. Since the normal and shear interface stresses are acting directly on the interface, they should be continuous across the interface. It should be pointed out that mesh refinements, interpretation of the results, and convergence check are done based on the fact that normal and shear stresses should be continuous across the interface.

In case of temperature dependent properties, the thermal strain will be written in incremental form for each $\mathrm{d}T$, then they will add up to get the right value of ε. For example, the variation of ε due to $\mathrm{d}T$ change in temperature is given as

$$\mathrm{d}\varepsilon = \alpha\big|_T(T - T_0) - \alpha|_{T-\mathrm{d}T}(T - \mathrm{d}T - T_0), \tag{8}$$

where T_0 is the reference temperature and is equal to zero.

3.2. Finite element analysis

The uncoated superalloy specimen has a thickness of 3.175 mm, the bond coat layer thickness is 24.15 μm, the oxide layer thickness is 24.15 μm, the ceramic layer (TBC) thickness is 127 μm, and the width of the specimen is 25.4 mm for the plane strain case (Fig. 2b). The properties of these four layers are given in Table 1. We analyzed a model case where the specimen was plasma sprayed in air with a thin zirconia–yttria (ZrO_2–8wt.%Y_2O_3) layer on a nickel–chromium–aluminum–zirconium bond coat, (Chang et al., 1987). The specimen was cooled down from a processing temperature of 1000°C to room temperature of 25°C. A general finite element code ABAQUS was used for numerical calculations.

3.3. Computational fracture analysis

ABAQUS was used to estimate *J*-integral values at crack tips for the interface cracks. The oxide scale volume growth can be accounted for as internal pressure. Previous work (Nusier and Newaz, 1998b) has shown that a small 50 MPa pressure can have significant effect.

4. Results and discussion

When the specimen was cooled down from a processing temperature of 1000°C to a temperature of 25°C and then elevated to a temperature of 1177°C, the stresses in bond coat and TGO were tensile stresses (refer to point 'b' in Figs. 3 and 4 respectively). Analysis showed that if the specimen were cooled from 1177°C to 25°C without considering the creep effect the final stress would be the point 'NC*' in Figs. 3 and 4 i.e. same

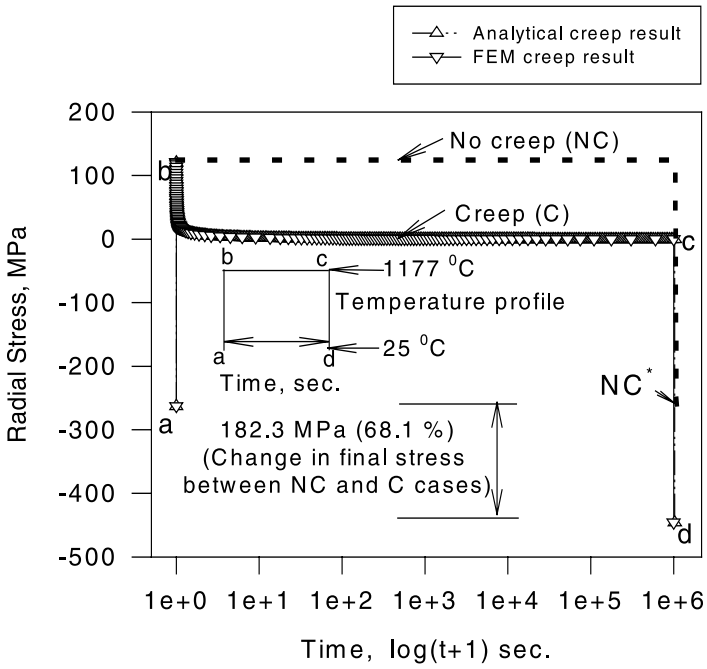

Fig. 3. Thermal loading cycle and corresponding stress versus time profile in bond coat for disk specimen. Analytical and FEM results match very well. (NC* represents the final value for NC analysis).

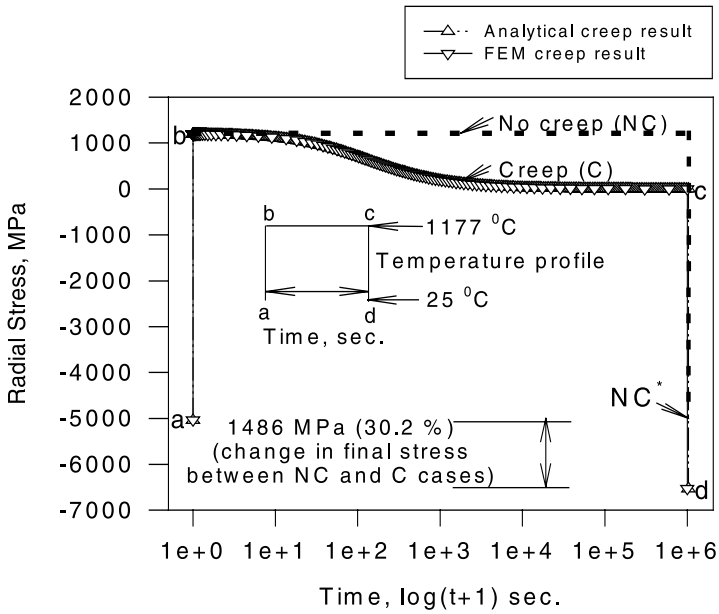

Fig. 4. Thermal loading cycle and corresponding stress versus time profile in oxide layer for disk specimen. Analytical and FEM results match very well. (NC* represents the final value for NC analysis).

stress as point 'a' in the corresponding figure. But due to creep the stress at that higher temperature (1177°C) decayed after a particular period of time. The specimen was then cooled from that point (refer to point 'c' in Figs. 3 and 4) but the final stresses were not at the point 'NC*' as mentioned above. The final stresses were below the point 'NC*' (refer to point 'd' in Figs. 3 and 4), which showed larger compressive stresses. This can be explained as at 1177°C due to creep the stresses decayed to zero in different layers of the superalloy system. It seems as if the processing temperature were 1177°C rather than 1000°C. As that was the case at point 'c' (refer to Figs. 3 and 4), obviously higher processing temperature would give higher residual stresses upon cooling to 25°C. This argument was verified analytically.

For the creep laws that have been used, the stresses in bond coat decayed very quickly compared to oxide layer. Fig. 3 is showing bond coat radial stress versus log time. To show the stresses at zero time the value 1 is added with each time scale for convenience. From Fig. 3 it can be shown that at elevated temperature the radial stress in bond coat decays to 1% at time 62 s. Fig. 4 is showing TGO layer radial stress versus log time. Here also to show the stresses at zero time the value 1 is added with each time scale for convenience. From Fig. 4 it can be shown that at elevated temperature the radial stress in TGO layer decays to 1% at time 8.09×10^5 s. The specimen was held at elevated temperature for 1×10^6 s to get radial stress in the TGO close to zero. Then it was cooled to temperature 25°C. The residual radial stresses in bond coat and TGO layer were found 68% and 30% respectively more than if there were no creep. From analytical investigation it has been found that if the specimen was cooled to 25°C before the complete decay of stresses at holding temperature, the final stresses would be at a level between points 'a' and 'd' of Figs. 3 and 4.

In the asperity analysis a parametric study was carried out in which the effect on interface stresses due to variation in three wave amplitudes, and four wavelengths representing different levels of asperity were considered. In this study the material properties were considered to be temperature dependent, so that the results will be more practical. Fig. 5 shows the interface normal stress versus radial position for three wave amplitude (2.413, 1.2065, 0.60325 μm) and one wavelength (31.75 μm), while Fig. 6 shows the interface shear stress for same case. These values of undulation heights were obtained from experimental

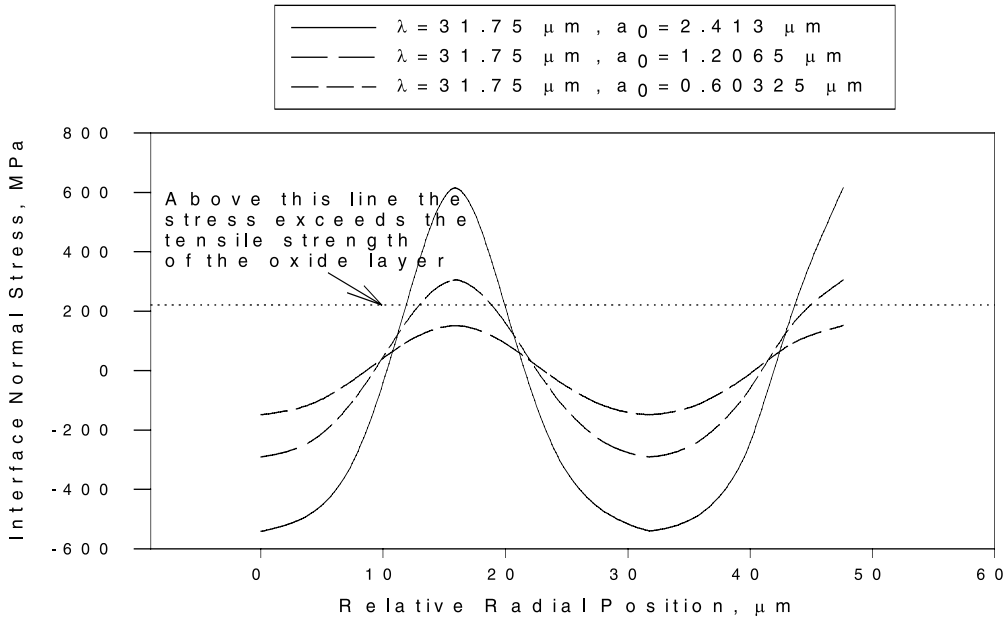

Fig. 5. Interface normal stress versus radial position.

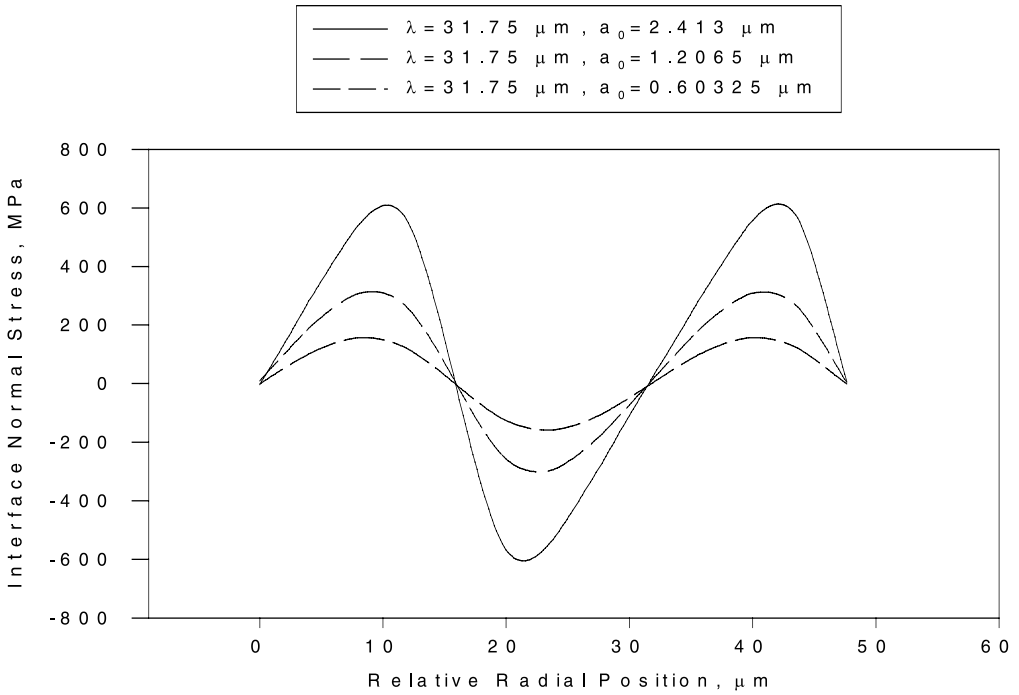

Fig. 6. Interface shear stress versus radial position.

observation. From these figures it is clear that normal and shear stresses followed the trigonometric functions sine and cosine, respectively. Small wavelength and high wave amplitude gives a high normal and shear stresses. The highest normal stress occurred at the peaks of rough interface, while the highest shear stress occurred at the mean line of the rough interface.

For the case of 2.413 μm wave amplitude and 31.75 μm wavelength, the peak value of interface normal stress reaches a value of approximately 600 MPa, which exceeds the oxide tensile strength (≅215 MPa). For a radial length of about 10 μm, the interface normal stress is exceeding the tensile strength of the oxide layer, so a crack of 10 μm will be created at the peaks of the rough interface. Since at the tips of these cracks, the normal stresses are still high, one can expect that these cracks will propagate to greater lengths. On the other hand, the shear stress has a peak value at the mean line of the rough interface, for a case similar to the previous one, cracks of 15 μm or longer will be created at the mean line of the rough interface, since the shear strength of the oxide/bond interface is approximately 70 MPa. Figs. 7 and 8 show that the variation of normal stress versus wave amplitude and the inverse of the wavelength are close to linear. The case of shear stresses shows similar trend.

Based on the previous discussion the following empirical formulae seems to be a good fit for normal and shear stresses:

$$\sigma_{nn} = \frac{2\pi a_0}{\lambda}\left(\frac{1}{2E^{o}} + \frac{1}{2E^{b}}\right)^{-1} \varepsilon \sin\left(\frac{2\pi r}{\lambda}\right), \qquad \sigma_{nt} = \frac{2\pi a_0}{\lambda}\left(\frac{1}{2E^{o}} + \frac{1}{2E^{b}}\right)^{-1} \varepsilon \cos\left(\frac{2\pi r}{\lambda}\right), \tag{9}$$

where ε is the thermal strain and can be calculated by means of Eq. (8), v is Poisson's ratio, E is modulus of elasticity, and superscripts o and b corresponding to oxide and bond coat layers respectively. The sine and cosine functions chosen for the surface function reflect the physical features of the surface. However, their selection need not be unique and final results will be affected based on the choice of the surface function.

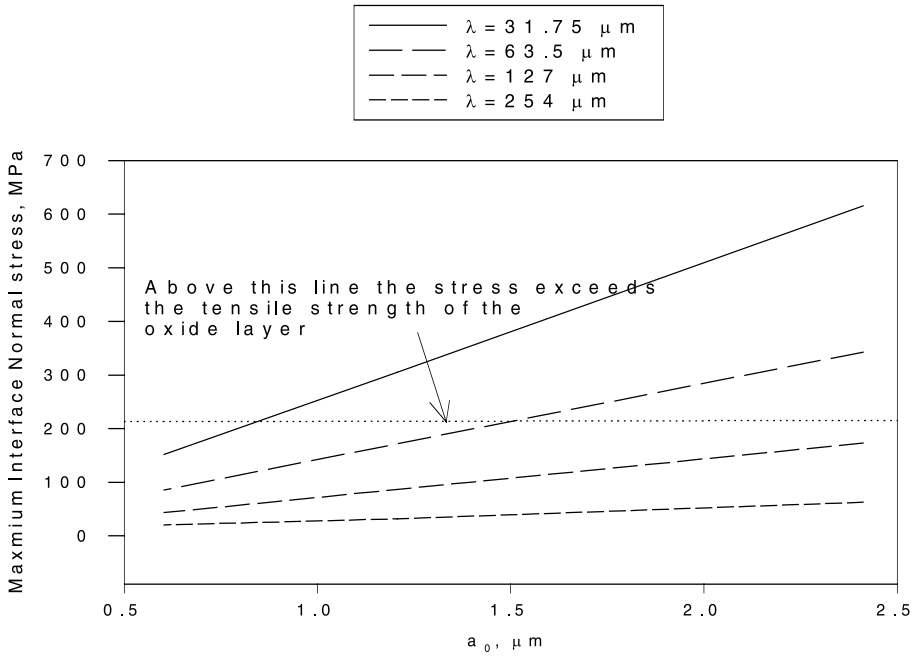

Fig. 7. Maximum interface normal stress versus wave amplitude.

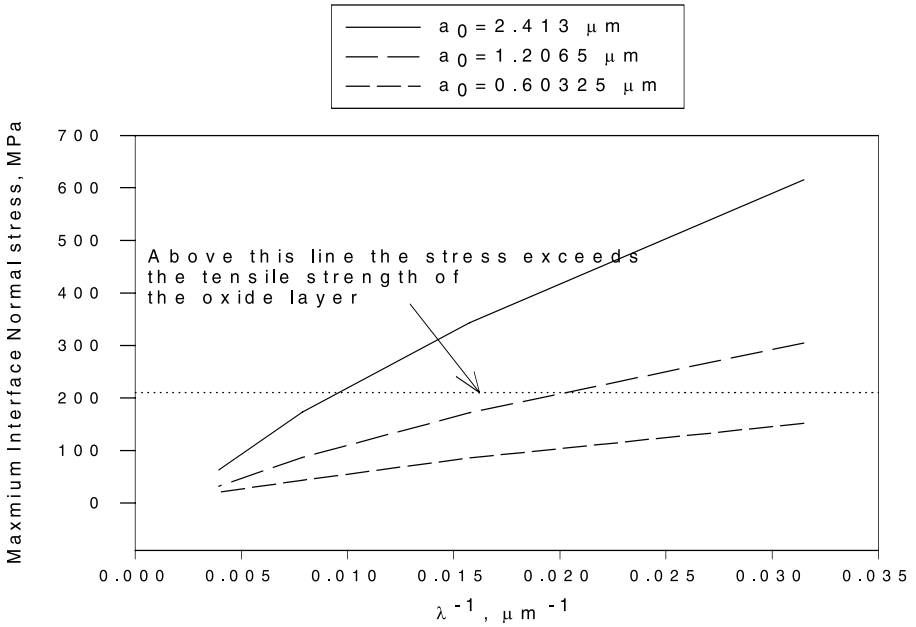

Fig. 8. Maximum interface normal stress versus the inverse of the wave length.

Fig. 9 shows the variation of *J*-integral with delamination radius from numerical analysis. From this figure one can obtain the conditions when the crack will propagate. From literature the critical energy release rate is 35 J m/m^2 based on alumina toughness. For a value of 35 J m/m^2, and a delamination radius of four times the TBC thickness, the crack will propagate at induced pressure value equivalent to 200 atm. (≈20 MPa). This value is easy to develop due to volume increase because of oxide layer growth. Also, based

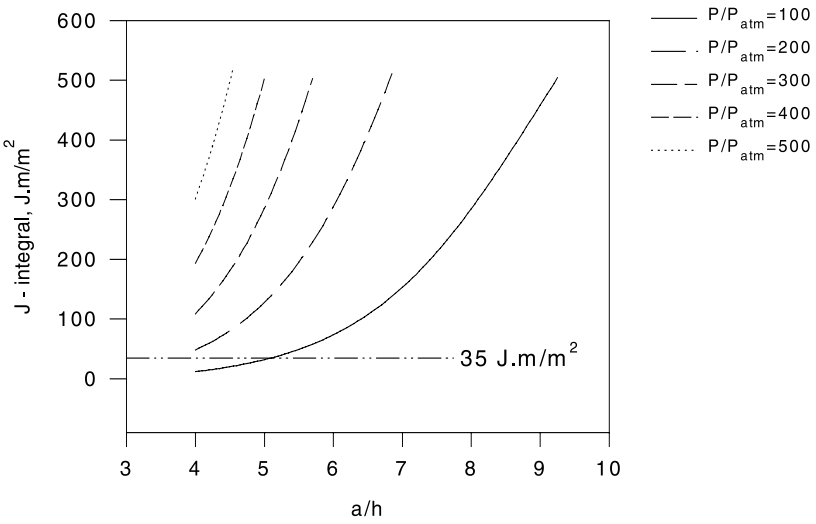

Fig. 9. Variation of *J*-intergal versus delamination radius at different pressure ratio. Temperature dependent material properties are used in the analysis (numerical results).

on finite element analysis conducted by the authors for this system with a wavy interface, the results shows that an axial stress of 250 MPa can be developed for a sine wave interface with amplitude of 2.4 μm and wavelength of 127 μm. These values are practical for this system (Nusier and Newaz, 1998b).

5. Summary and conclusions

1. Radial stress in the TGO layer is substantially higher compared with the radial stress in the bond coat (one order of magnitude) and plays a critical role in early damage initiation in TBC coated superalloy system. Compressive stress can be high (~6400 MPa) indicating that microcracking within the TGO layer is a definite possibility since TGO compressive strength for pure Al_2O_3 is ~3860 MPa (for zero porosity 100% polycrystalline alumina)
2. Using creep laws from literature for bond coat and TGO, a 30% increase in compressive stress is expected in TGO. This enhances the possibility of early damage initiation in TGO/bond coat interface based on the compressive strength of pure Al_2O_3 as given in Eq. (1).
3. At the wavy interface, the normal and shear stresses followed the trigonometric functions sine and cosine, respectively. Small wavelength and high wave amplitude gives high normal and shear stresses. The highest normal stress occurred at the peaks of rough interface, while the highest shear stress occurred at the mean line of the rough interface.
4. For the case of 2.413 μm wave amplitude and 31.75 μm wavelength, the peak value of interface normal stress reaches a value of approximately 600 MPa, which exceeds the oxide tensile strength (≅215 MPa).
5. For a value of 35 J m/m^2, and a delamination radius of four times the TBC thickness, the crack will propagate at induced pressure value equivalent to 200 atm. (≈20 MPa)

Acknowledgements

Funding for this research was provided through a grant (#F49620-98-1-0390) from the Air Force Office of Scientific Research (AFOSR). Dr. H. Thomas was the program monitor. Discussion and interaction with Dr. P.K. Wright of GEAE is gratefully acknowledged.

References

Brindley, W.J., Whittenberger, J.D., 1993. Stress Relaxation of Low Pressure Plasma-Sprayed NiCrAlY Alloys. Materials Science and Engineering A163, 33–41.

Carapella, E.E., Hyer, M.W., Griffin, O.H., Maahs, H.G., 1994. Micromechanics of Crenulated Fibers. Journal of Computational Maths 28 (14), 1322–1346.

Chai, H., 1990. Three-Dimensional Fracture analysis of Thin-Film Debonding. International Journal of Fracture 46, 237–256.

Chang, G.C., Phucharoen, W., Miller, R.A., 1987. Finite Element Thermal Stress Solutions for Thermal Barrier Coatings. Surface and Coatings Technology 32, 307–325.

Clarke, J.M., Barnes, J.F., 1971. Stress Redistribution Caused by Creep In A Thick Walled Circular Cylinder Under Axial and Thermal Loading. In: Smith, A.I., Nicolson, A.M. (Eds.), Advances in Creep Design, Wiley, New York, pp. 387–420.

Evans, H.E., Strawbridge, A., Carolan, R.A., Ponton, C.B., 1997. Creep Effects On The Spallation of an Alumina Layer from a NiCrAlY Coating. Materials Science and Engineering A 225, 1–8.

Lin, H.T., Becher, P.F., 1990. Journal of American Ceramic Society 73, p. 1378.

Newaz, G.M., Nusier, S.Q., Chaudhury, Z.A., 1998a. Damage Accumulation Mechanisms in Thermal Barrier Coatings. ASME, Journal of Engineering Materials and Technology 120 (2), 149–153.

Nusier, S.Q., Newaz, G.M., 1998b. Analysis of Interfacial cracks in a TBC/Superalloy System Under Thermomechanical Loading. Journal of Engineering for Gas Turbines and Power 120, 813–819.

Nusier, S.Q., Newaz, G.M., 1998c. Crack Initiation In Thermal Barrier Coatings Due to Interface Asperity. Proceedings of the Eighth Japan–U.S. Conference on Composite Materials, September 1998, pp. 417–426.

Ryan, R.L., McCafferty, E., 1995. Rupture of an Oxide Blister. Journal of Electrochemical Society 142 (8), 2594–2597.

Wan, K., Mai, Y., 1995. Fracture Mechanics of a Shaft-Loaded Blister of Thin Flexible Membrane on Rigid Substrate. International Journal of Fracture 74, 181–197.